

Nonlinear Analysis of a Single Stage Pressure Relief Valve

Gábor Licskó *

Alan Champneys †

Csaba Hős ‡

Abstract—A mathematical model is derived that describes the dynamics of a single stage relief valve embedded within a simple hydraulic circuit. The aim is to capture the mechanisms of instability of such valves, taking into account both fluid compressibility and the chattering behaviour that can occur when the valve poppet impacts with its seat. The initial Hopf bifurcation causing oscillation is found to be either super- or sub-critical in different parameter regions. For flow speeds beyond the bifurcation, the valve starts to chatter, a motion that survives for a wide range of parameters, and can be either periodic or chaotic. This behaviour is explained using recent theory of nonsmooth dynamical systems, in particular an analysis of the grazing bifurcations that occur at the onset of impacting behaviour.

Keywords: relief valve, chaos, grazing, piecewise-smooth

1 Instabilities in relief valves

Hydraulic relief valves are widely used to limit pressure in hydraulic power transmission and control systems. There is a rich literature that describes their usage in hydraulic circuits and gives information on their design and application. A brief overview on elements of hydraulic systems can be found in the book of Bolton [1]. More detailed information on hydraulic elements can be found in Steward's book [10] together with lots of industrial examples mostly from the area of manufacturing. Kay [8] focuses more on industrial pneumatics again with many application examples.

In hydraulic circuits that are in steady operating conditions, and the constant flow rate input of the system is less than the delivered flow rate of the pump then the difference will flow through the by-pass line secured by a relief valve. Such situations arise when economic operation is not so important. The other case when relief valves interact in most of the hydraulic equipments (such as those installed on excavators, etc.) is when transient

phenomena occur (e.g. the scoop sticks in a rocky layer below the soil) and the pressure rises much above the tolerable limit. The relief valve has to intervene and limit the pressure so that other parts of the circuit are not damaged. These are the main reasons why designers of such systems have to insert pressure limiters into the circuit.

Figure 1 shows a so called direct operated pressure relief valve. The simplest configuration of such a relief valve is when an orifice is closed by a poppet or similar element. The closing force can be adjusted by pre-stressing a spring that presses the poppet towards the valve seat. This force divided by the cross-sectional area of the orifice also represents the opening pressure, the threshold at which the safety valve will come into operation.

There are numerous examples in industry where these kinds of valves can vibrate when their equilibria lose stability and many researchers have been interested in the investigation of this phenomenon. As far back as the 1960's researchers suspected that the piping to and from the relief valve cannot be neglected. Kasai [7] carried out a very detailed investigation of a simple poppet valve and he deduced a stability criterion analytically. He also proposed that circumstances other than just nonlinearity such as the poppet geometry or the change in the oil temperature can also lead to stability loss. Moreover he performed experiments and found good coincidence with his analytical results. Thomann [11] was also interested in the analysis of a pipe-valve system. He used a simple poppet type valve but analysed how different poppet geometries affect the stability. He investigated a conical

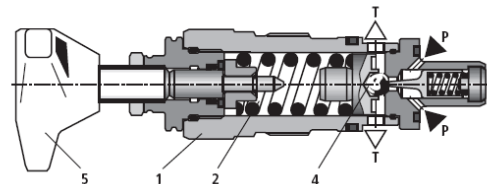


Figure 1: Direct operated pressure relief valve (1 - valve housing; 2 - spring; 4 - poppet; 5 - adjusting wheel; P - inlet; T - outlet) (image source: <http://www.boschrexroth.com/>).

*Department of Applied Mechanics, Budapest University of Technology and Economics, licsko@mm.bme.hu

†Department of Engineering Mathematics, University of Bristol, A.R.Champneys@bristol.ac.uk

‡Department of Hydrodynamic Systems, Budapest University of Technology and Economics, csaba.hos@hds.bme.hu

and a cylindrical poppet together with conical or cylindrical seats, and their combination. Hayashi et al.[5, 6], built up a model with a constant supply pressure and investigated the valve's response and stability, finding that a Hopf bifurcation occurs.

This report shall consider a modern analysis of relief valve chatter using ideas from nonsmooth dynamical systems. See e.g. [2]. A simple set-up will be chosen that considers the dynamics of the valve in the context of a hydraulic circuit.

The rest of the work is organized as follows: first in Section 2 we present a mathematical model that is believed to accurately describe the behaviour of a pressure relief valve. In Subsection 2.2 we continue with a linear stability analysis of the derived equations and try to show that in certain cases self-excited limit cycle vibration occur. In Subsection 2.3 we carry out a nonlinear analysis, since we wish to determine the stability of the limit cycle found. We will also be interested in the possible change of this stability by varying parameters along the critical curve where dynamical stability loss occurs.

Exciting nonsmooth phenomena can be exhibited by these kinds of mechanical systems when moving parts collide with standing ones. Such impacts can affect the system's behaviour globally and we wish to understand more about how nonsmooth bifurcations occur in this particular example (e.g. grazing bifurcation). Towards this we will use numerical techniques in Section 3 and compute bifurcation diagrams using an appropriate simulator. Then in Section 4 we will also try to investigate the dynamics of grazing analytically.

2 The mathematical model

Figure 2 depicts a sketch of the analyzed system, which is similar to those used by Kasai [7] and Hayashi [6].

The system consists of a hydraulic aggregate and a safety valve connected by fluid conveying tubes, the fluid is redirected into an oil chamber after leaving the test valve. The oil is supplied by an aggregate that consist of the gear pump and an additional safety valve for the protection of the system. This hydraulic aggregate provides the system the flow rate Q_p . However, due to compressibility of the fluid and elasticity of the tubes, the flow rate at the test valve can be different from that one at the exit to the pump. To model the compressibility effects, a hypothetical chamber is added whose volume is equal to the total volume of oil in the system. This chamber will represent the stiffness of our system.

The mass balance equation for this chamber (labeled 3 in Fig. 2) can be written as follows:

$$\frac{d}{dt}(\rho V) = \rho [Q_p - Q(x, p)], \quad (1)$$

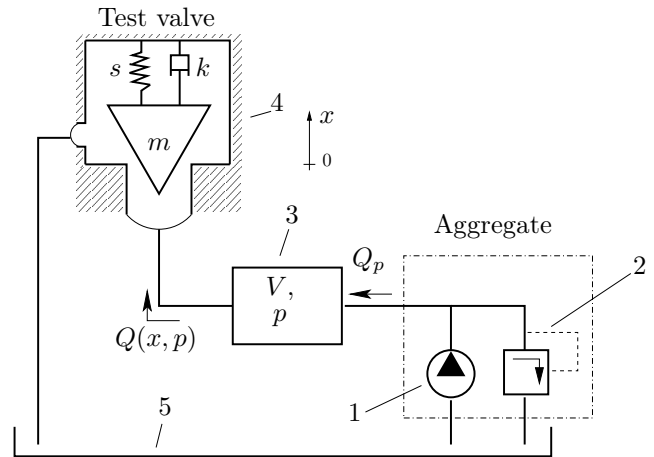


Figure 2: Schematic diagram of a simple hydraulic system consisting of a gear pump (1), a relief valve (2), a hypothetical chamber (3) that represents the total tubing in a real system, the pressure relief valve (4) we wish to test and an oil tank (5).

where V represents the total volume of the system, ρ denotes the density of the fluid and p is the oil pressure at the relief valve, Q_p is the flow rate delivered by the pump and Q is the flow rate through the valve, which is a function of both the valve displacement x and the system pressure p :

$$Q(x, p) = A(x)C_d\sqrt{\frac{2}{\rho}p}. \quad (2)$$

Let us suppose that the valve is partly open. The flow-through area between the valve body and the seat will be calculated via the simplification that the normal distance h of the cone to the valve seat (see Fig.3) is revolved around the symmetry axis of the cone along the circumference at an average radius. With these assumptions, we obtain

$$A(x) = d\pi h = (D - h \cos \alpha)\pi h,$$

where d and D are defined in the figure and α is the semi-angle of the cone. With the substitution of $h = x \sin \alpha$ we finally obtain:

$$A(x) = (D - x \sin \alpha \cos \alpha)\pi x \sin \alpha = (1 - \frac{x}{D} \sin \alpha \cos \alpha)D\pi x \sin \alpha. \quad (3)$$

See Figure 3 for the geometry of the valve's interior. With the assumption that the fluid is barotropic, i.e. its density depends only on the pressure, the left-hand side of Eq.(1) can be written as follows:

$$\frac{d}{dt}(\rho V) = V \frac{d\rho}{dt} + \rho \frac{dV}{dt} = V \frac{d\rho}{dp} \frac{dp}{dt} = V \frac{\rho}{E} \frac{dp}{dt},$$

where a stands for sonic velocity: $a^2 = \frac{dp}{d\rho} = \frac{E}{\rho}$. The dynamics of the valve body is described by Newton's second

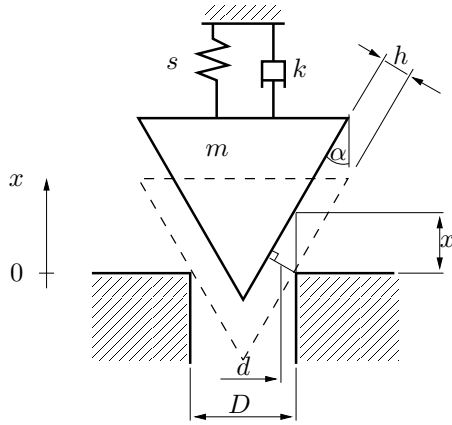


Figure 3: Geometry of the valve for calculation of the relationship between the effective orifice area $A(x)$ and displacement x .

law, together with the usual impact law modelling the energy loss of the impact via the restitution coefficient r . Finally, the system's behaviour is described by the following system of ordinary differential equations (ODEs):

$$\begin{aligned} \dot{x} &= v, \\ \dot{v} &= \frac{pA}{m} - \frac{k}{m}v - \frac{s}{m}(x + x_0), \\ \dot{p} &= \frac{E}{V} \left[Q_p - A(x)C_d \sqrt{\frac{2}{\rho}p} \right] \quad \text{and} \\ v^+ &= R(v^-) = -rv^-. \end{aligned} \quad (4)$$

Here x and v denote the displacement and velocity of the valve body, k is the damping coefficient, s is the spring stiffness, m is the total mass of the moving parts and x_0 denotes the pre-stress of the spring. A is the area on which the fluid force originating from the pressure within the system acts, p denotes the excess pressure in the system compared to atmospheric pressure p_0 (the pressure in the oil tank) and E is the reduced modulus of elasticity of the system after taking account of the oil compressibility and the expansion of the tubes. Q_p denotes the oil flow rate generated by the gear pump, V is the overall volume of the system filled with oil. $C_d(Re)$ is a discharge coefficient at the valve inlet which in general depends on the Reynolds number, although this dependence will be neglected in our subsequent analytical and numerical investigation. $A(x)$ denotes the effective orifice cross-sectional area when the valve is partly open and ρ is the density of the oil respectively. The expression of the orifice cross-sectional area $A(x)$ shown in Eq. (3) is very complicated so it is worth to linearise and write $A(x) = c_1x$, where c_1 refers to the linear coefficient that describes the cross sectional area of the orifice as the function of the valve stem displacement. Since we experienced very small displacements during the experiments, the linearisation is believed to be an accurate approximation and so we can

restrict the nonlinearity to the third equation.

The last equation represents a simple impact law where v^- is the velocity before impact, v^+ is the velocity after impact and r is the coefficient of restitution.

2.1 Dimensionless equations

In order to treat the system in a more convenient way let us transform the equations into a non-dimensional form. We introduce the dimensionless variables $y_i(\tau)$ $i = 1, \dots, 3$, where:

$$\begin{aligned} \tau &= \frac{t}{t_{ref}}, \quad y_1 = \frac{x}{x_{ref}}, \quad y_2 = \frac{t_{ref}}{x_{ref}}v, \quad y_3 = \frac{p}{p_{ref}}, \\ t_{ref} &= \sqrt{\frac{m}{s}}, \quad p_{ref} = p_0 \quad \text{and} \quad x_{ref} = \frac{Ap_0}{s}. \end{aligned}$$

Eq.(4) can then be written in the nondimensional form

$$\begin{aligned} y_1' &= y_2 \\ y_2' &= -\kappa y_2 - (y_1 + \delta) + y_3 \\ y_3' &= \beta (q - \sqrt{y_3}y_1) \\ y_2^+ &= -ry_2^-, \end{aligned} \quad (5)$$

where the nondimensional parameters are

$$\begin{aligned} \kappa &= \frac{k}{m} \sqrt{\frac{m}{s}} \quad (\text{nondimensional damping coefficient}) \\ \beta &= \frac{E}{V} \frac{C_d c_1 A}{\rho} \sqrt{\frac{2p_0 m}{\rho s}} \quad (\text{nondimensional stiffness param.}) \\ \delta &= \frac{s x_p}{A p_0} \quad (\text{nondimensional pre-stress parameter}) \\ q &= \frac{Q_p}{C_d c_1 \frac{A p_0}{s} \sqrt{2 \frac{p_0}{\rho}}} \quad (\text{nondimensional flow rate}). \end{aligned}$$

Table 1 contains the physical parameters of the test rig

Par.	Description	Value
m	mass of moving parts	0.45 [kg]
s	stiffness of valve spring	15000 [N/m]
k	damping coefficient	10-100 [Ns/m]
p_0	reference pressure	1e5 [Pa]
A	valve inlet cross section	1.767e-4 [m ²]
E	bulk modulus	0.435e9 [Pa]
V	total system volume	4.42e-4 [m ³]
C_d	discharge coefficient	0.86 [-]
ρ	medium density	870 [kg/m ³]
c_1	orifice opening parameter	0.0408 [m ²]

Table 1: Physical parameters of the test rig used for calculation of the nondimensional parameters.

built up in the laboratory of the Department of Hydrodynamic Systems at the Budapest University of Technology and Economics. We use these to calculate the nondimensional parameters. We obtain that $\kappa = 1.2172$ [-],

$\beta = 19.5062 [-]$ and $\delta = 10 [-]$ corresponds to an opening pressure of $p_{opening} = 10 [bar]$ of the relief valve. From now on let us simplify the calculation and use $\kappa = 1.25 [-]$, $\beta = 20 [-]$ and $\delta = 10 [-]$ instead. The nondimensional damping coefficient is only a rough approximation as it is highly nontrivial how to estimate this parameter.

2.2 Linear stability analysis

When investigating dynamical systems we are interested in finding equilibria and determining their stability. Therefore our first step will be to solve the governing equations when all the derivatives on the left-hand-side are zero. We then try to find cases when dynamical stability loss occur, e.g. when self excited oscillations arise. In these cases a pair of complex conjugate eigenvalues of the system cross the imaginary axis with non-zero velocity, e.g. their real part changes sign and become positive. We will search for a stability criterion using the system's characteristic equation.

2.2.1 Equilibrium of the system

To calculate the equilibrium of the system we shall put the equations (5) in the form $y' = f(y) = 0$. With the substitution $\sqrt{y_3} = z$ we obtain the following third order equation

$$z(z^2 - \delta) - q = 0. \tag{6}$$

We find that the real solution is

$$\begin{aligned} y_1 &= y_3 - \delta, \\ y_2 &= 0, \\ y_3 &= \frac{\left[(108q + 12\sqrt{-12\delta^3 + 81q^2})^{2/3} + 12\delta \right]^2}{36 \left(108q + 12\sqrt{-12\delta^3 + 81q^2} \right)^{2/3}}. \end{aligned}$$

For simplicity of the analytical calculations let us neglect the nondimensional prestress ($\delta = 0$) so that the equilibrium of Eq.(5) simplifies to

$$(y_1^e, y_2^e, y_3^e) = (q^{2/3}, 0, q^{2/3})$$

After linearisation around this equilibrium the Jacobian of the system is:

$$J = \begin{pmatrix} 0 & 1 & 0 \\ -1 & -\kappa & 1 \\ -\beta q^{1/3} & 0 & -\frac{1}{2}\beta q^{1/3} \end{pmatrix}, \tag{7}$$

which has the characteristic equation

$$\lambda^3 + a_2\lambda^2 + a_1\lambda + a_0 = 0, \tag{8}$$

where $a_2 = \kappa + \frac{1}{2}\beta q^{1/3}$, $a_1 = 1 + \kappa\beta\frac{1}{2}q^{1/3}$ and $a_0 = \frac{3}{2}\beta q^{1/3}$. Now let us to substitute $\lambda = 0$ into Eq.(8) and conclude that steady stability loss (a fold bifurcation) can occur when following condition is true:

$$a_0 = \frac{3}{2}\beta q^{1/3} = 0.$$

Of course this case is meaningless, since $\beta > 0$ and we always assume a flow rate greater than zero.

We furthermore expect that the system undergoes a dynamical stability loss, so now we substitute $\lambda = i\omega$ into Eq.(8) in order to obtain the criterion $a_1a_2 = a_0$ for the Hopf-bifurcation. From this condition we can compute the curve of stability loss for the nondimensional damping coefficient as the function of the nondimensional flow rate analytically:

$$\kappa = \frac{-\beta^2 q^{2/3} - 4 + \sqrt{\beta^4 q^{4/3} + 40\beta^2 q^{2/3} + 16}}{4\beta q^{1/3}} \tag{9}$$

Figure 4(a) shows the curve as a stability diagram. Here we substituted $\beta = 1$ into the equation above, results for other β values are qualitatively similar. The vibration frequency at the critical points (i.e. on the curve) can also be derived from the same condition. We obtain $\omega = \sqrt{a_1}$, where a_1 is the coefficient of λ in the characteristic polynomial. With the transformation to dimensional coordinates we reach to the diagram shown in Figure 4(b) for the system's vibration frequencies. Here we used parameters that corresponds to the test equipment again (see Table 1). Figure 5. depicts the same stability diagram as 4(a) but in this case with physical parameters. We notice that the curve begins at the origin and has a local extremum (maximum) at $Q_p = 0.05 [l/min]$. If we assume, that our test valve can be characterized by a viscous damping coefficient of $k = 20 [Ns/m]$ (marked with a red line on Fig.5) then the unstable region obtained from the diagram is below $Q_p \cong 0.25 [l/min]$. Here again we should mention that measuring the damping ratio is one of the most difficult tasks when investigating dynamical systems experimentally.

2.3 Nonlinear analysis

Having found the presence of a Hopf bifurcation, we are interested in the stability of the limit cycle. To do this, we will apply the normal form theory described for example in [4] and use the centre manifold reduction. We then compute the *first Lyapunov coefficient* to determine stability. We also compute the coefficient along the stability curve obtained in Section 2.2 to see how it will change when varying some parameter. For simplicity we stick to the case $\delta = 0$.

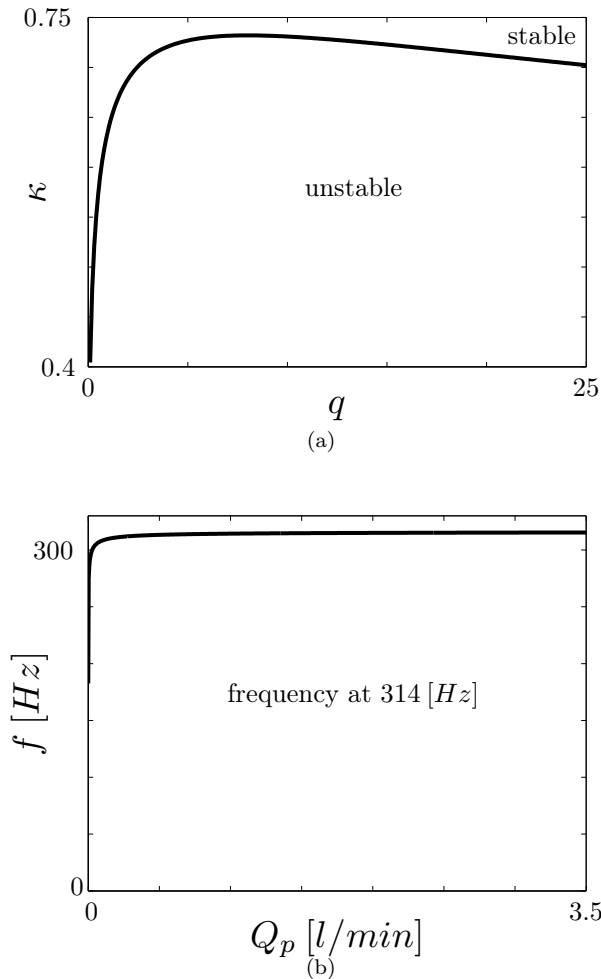


Figure 4: Stability diagram for the nondimensional damping coefficient with respect to the nondimensional flow rate (a), the vibration frequency for the test system is expected to be at 314 [Hz] (b), using parameters in Table 1.

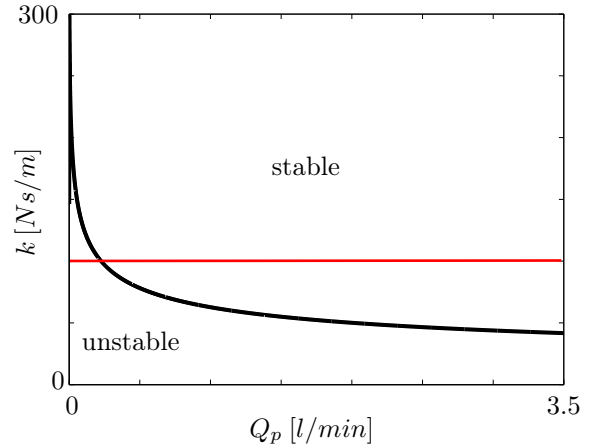


Figure 5: Stability diagram for the laboratory test valve assuming $k = 20$ [Ns/m] (red line)

2.3.1 Normal form transformation

First we substitute $\chi = \beta q^{1/3}$ into Eq. (7) to simplify the calculation. With this we can eliminate the parameter β from the equations. Now Eq. (7) can be written

$$J = \begin{pmatrix} 0 & 1 & 0 \\ -1 & -\kappa & 1 \\ -\chi & 0 & -\chi/2 \end{pmatrix}. \quad (10)$$

We next compute the three eigenvectors of the Jacobian that we will use for the linear transformation to appropriate coordinates. They are

$$s_1 = \begin{pmatrix} 1 \\ i\omega \\ 1 - \omega^2 - \kappa i\omega \end{pmatrix}, \quad s_2 = \begin{pmatrix} 1 \\ -i\omega \\ 1 - \omega^2 - \kappa i\omega \end{pmatrix}$$

$$s_3 = \begin{pmatrix} 1 \\ -\kappa - \chi/2 \\ \kappa\chi/2 + \chi^2/4 + 1 \end{pmatrix}.$$

These eigenvectors correspond to the case when two purely imaginary and one real eigenvalues exist. Specifically: $\lambda_1 = i\omega$, $\lambda_2 = -i\omega$ and $\lambda_3 = -\kappa - \chi/2$.

The normal form transformation is a coordinate transformation from the original coordinates (y_i , $i = 1 \dots 3$ in our case) to coordinates (ξ as they will appear later) laying on a polynomial approximation to the so-called centre manifold. The local dynamics of the system on the centre manifold are then topologically equivalent to those in the phase space and so we can analyse stability by reducing the number of coordinates from the three-dimensional space to the plane.

The linear part transformation is carried out by a matrix

of the form

$$T = \begin{pmatrix} Re(s_1) & Im(s_1) & s_3 \end{pmatrix} = \begin{pmatrix} 1 & 0 & 1 \\ 0 & \omega & -\kappa - \chi/2 \\ 1 - \omega^2 & -\kappa\omega & \kappa\chi/2 + \chi^2/4 + 1 \end{pmatrix}.$$

Here the columns of T represent the real and imaginary parts of the first and the real third eigenvector. Our aim by choosing the elements of the transformation matrix is to obtain a system with real parameters after the transformation.

Before being able to do the transformation it is simplest to replace all nonlinear equations with their third order Taylor expansion around the equilibrium to put the system into the following form

$$\eta' = J\eta + p_3(\eta),$$

where J is the linear coefficient matrix, e.g. the Jacobian of the system and p_3 contains all the higher order terms. Here we also consider small disturbances around the equilibrium and put therefore $\eta = y - y_0$ into the equations.

The coordinate transformation is then following

$$\eta = T\xi, \tag{11}$$

and the equation will have the form

$$T\xi' = AT\xi + p_3(T\xi).$$

We can write such a system in first order form as

$$\xi' = \underbrace{T^{-1}AT}_B \xi + H(\xi),$$

or more conveniently in matrix form

$$\begin{pmatrix} \xi_1' \\ \xi_2' \\ \xi_3' \end{pmatrix} = \begin{pmatrix} 0 & \omega & 0 \\ -\omega & 0 & 0 \\ 0 & 0 & -\lambda_3 \end{pmatrix} \begin{pmatrix} \xi_1 \\ \xi_2 \\ \xi_3 \end{pmatrix} + \begin{pmatrix} H_1(\xi) \\ H_2(\xi) \\ H_3(\xi) \end{pmatrix}. \tag{12}$$

Note that elements of the nonlinear vector $H(\xi)$ may contain any combination of products of the transformed coordinates.

2.3.2 Centre manifold reduction

A problem arises when we wish to apply normal form theory to our three-degrees-of-freedom system, since it is only applicable for systems of two degrees of freedom. Therefore we express the third coordinate ξ_3 with the other two as a second-order Taylor series

$$\xi_3 = h_{11}\xi_1^2 + h_{12}\xi_1\xi_2 + h_{22}\xi_2^2 + \mathcal{O}(\xi^3) \tag{13}$$

We now need to find equations for the coefficients h_{11} , h_{12} and h_{22} . The idea we will use is to compute the derivative

of Eq. (13) and make it equal to the third equation of our system in Eq. (12). Then we can express these coefficients with those used for the third-order approximation of the nonlinear equation in the following way

$$\begin{aligned} 2h_{11}\xi_1 \underbrace{\xi_1'}_{\omega\xi_2} + h_{12}(x_1'\xi_2 + \xi_1 \underbrace{\xi_2'}_{-\omega\xi_1}) + 2h_{22}\xi_2\xi_2' &= \\ &= \lambda_3 (h_{11}\xi_1^2 + h_{12}\xi_1\xi_2 + h_{22}\xi_2^2) + \\ &\quad + \underbrace{H_{311}\xi_1^2 + H_{312}\xi_1\xi_2 + H_{322}\xi_2^2}_{H_3(\xi_1, \xi_2)} \end{aligned}$$

Here we can substitute ξ_1' and ξ_2' from the first two equations of Eq. (12) as shown. This yields a linear system for the unknown vector $h = (h_{11} \ h_{12} \ h_{22})^T$

$$\begin{pmatrix} -\lambda_3 & -\omega & 0 \\ 2\omega & -\lambda_3 & -2\omega \\ 0 & \omega & -\lambda_3 \end{pmatrix} \begin{pmatrix} h_{11} \\ h_{12} \\ h_{22} \end{pmatrix} = \begin{pmatrix} H_{311} \\ H_{312} \\ H_{322} \end{pmatrix}$$

Now we know all the coefficients for the second order expression of our third coordinate ξ_3 that we can substitute into the first two equations of Eq. (12) and collect all the coefficients of the higher order terms. These we have to substitute into the so called *Bautin formula* [9] to obtain the value for the first Lyapunov coefficient. The formula we will use is as follows:

$$\begin{aligned} l(0) &= \frac{1}{8} \frac{1}{\omega} [(a_{20} + a_{02})(-a_{11} + b_{20} - b_{02}) + \\ &\quad (b_{20} + b_{02})(a_{20} - a_{02} + b_{11})] \\ &\quad + \frac{1}{8} [3a_{30} + a_{12} + b_{21} + 3b_{03}], \end{aligned}$$

where a_{ij} and b_{ij} ($i+j = 2, 3$) are coefficients of the higher order terms in the transformed equations. If $l(0) < 0$ then the Hopf bifurcation is supercritical, e.g. a stable limit cycle is born, and if $l(0) > 0$ then the bifurcation is subcritical and the limit cycle will be non-attracting.

2.3.3 Results

Figure 6 shows the Lyapunov coefficient along the stability curve obtained by the linear analysis. Note that there is a change in the sign around $\kappa = 0.67$, below which the second Hopf bifurcation point will become subcritical. Later we will present numerical continuation results showing this to be the case.

Now let we discuss further the values of the vibration frequency. As we obtained earlier in Section 2.2 there is an analytical expression for the frequency

$$\omega = \sqrt{a_1} = \sqrt{1 + \chi \frac{-\chi^2 - 4 + \sqrt{\chi^4 + 40\chi^2 + 16}}{8\chi}},$$

where $\chi = \beta q^{1/3}$.

The limits of ω for large and small flow rates are

$$\lim_{\chi \rightarrow 0} \omega = 1 \quad \text{and} \quad \lim_{\chi \rightarrow \infty} \omega = \sqrt{3}.$$

These analytical results are also clear to see in Figure 6. (Note the logarithmic scale on the figure.) This may suggest that the second Hopf point is quite far from the physical flow rate values that correspond to a lower range of χ . Now let us take a look at numerical continuation results

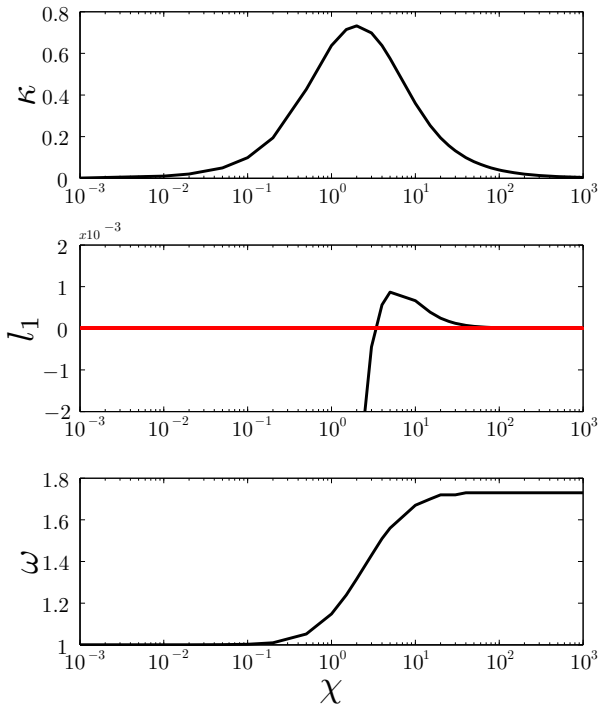


Figure 6: Stability curve (top), values of the Lyapunov coefficient along the stability curve (middle) and the vibration frequency (bottom) in logarithmic scale

for two different values of the damping coefficient. We used the program *AUTO* [3] (The program can be downloaded from <http://indy.cs.concordia.ca/auto/>). Fig. 7 shows the numerical continuation with $\kappa = 0.7$, where since $l(0) < 0$ in this region we have two supercritical Hopf bifurcation points. The solid lines represent the data from the *AUTO* calculation and the dashed lines show the analytical estimation of the vibration amplitude. For this we used the following formula:

$$r \approx \sqrt{-\frac{\sigma'_q(0)}{l(0)}(q - q^*)},$$

where r is the vibration amplitude in the transformed coordinates, $\sigma'_q(0)$ is the velocity at the critical point with which the complex conjugate eigenvalues are crossing the imaginary axis and $l(0)$ is the Lyapunov coefficient evaluated at the critical parameter value. q is the nondimensional flow rate and q^* is the flow rate at the critical point e.g. when we are on the stability curve. The crossing velocity $\sigma'_q(0)$ was computed numerically by solving

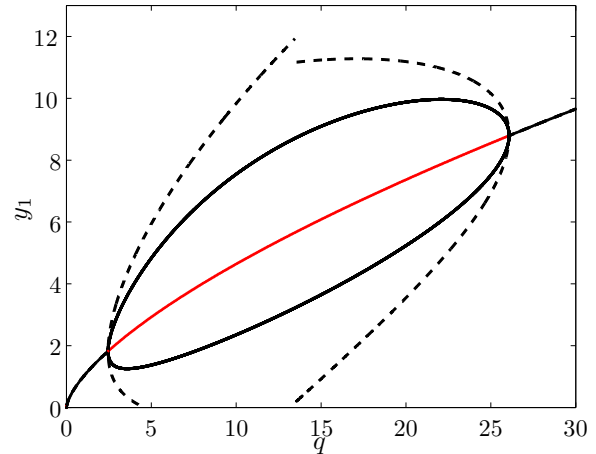


Figure 7: Continuation from the first Hopf point with $\kappa = 0.7$. Both points are supercritical. The dashed lines represent the analytical estimation, and the solid lines the results of *AUTO* computation.

the characteristic equation and estimating the derivative from the difference between values at discrete points. Afterwards we transformed r back to the real coordinates with Eq. (11)

$$\eta = T \begin{pmatrix} r \sin(\omega\tau) \\ r \cos(\omega\tau) \\ 0 \end{pmatrix}.$$

It is interesting to compare continuation diagrams with a reduced value of the damping coefficient in order to see, how the dynamics change around the critical points. Fig. 8 shows the neighborhood of the first Hopf bifurcation point at $q = 0.96$ with $\kappa = 0.4$. The stars mark the equilibria, circles represent the periodic solutions. Black markers are stable, red ones are unstable solutions. Here, the dashed line again shows the analytical estimation from the bifurcation point. We can see, that the first bifurcation point is supercritical, however the periodic solution reaches a fold point and turns back as an unstable periodic solution. Around $q = 0$ the continuation stopped with the lack of convergence.

In Fig. 9 we can see the second Hopf point at $q = 668.2$ from which an unstable periodic solution arises. The symbols and colors on this figure have the same meaning as on Fig. 8. Note that this value of the nondimensional flow rate is unphysically high for a real hydraulic system, since $q = 668.2 [-] \doteq 14500 [l/min]$ in the case of our particular test rig.

3 Global dynamics

In this section results of numerical methods are presented which were obtained from the simulation of the mathematical equations describing the model. Using this tech-

nique enables us to study the global dynamics of the system.

3.1 Numerical simulation

Numerical simulation is a simple and effective method for analysing dynamical systems and can be one step of a deeper investigation. It also enables us to treat systems with discontinuity, e.g. when the solution trajectory or its derivative is non continuous in the phase space. Of course there are several issues that we should take into consideration in order to obtain accurate results. For example the type of ODE solver. There are numerous computer environments that provide a numerical ODE solver such as some computer algebra packages or numerical mathematical packages. We chose this latter environment since it provides a wide range of solvers with adjustable error tolerance and gives us a convenient way to manipulate data and results using an effective programming language. It also enables us to use the so called *event handling* feature that is needed when treating impacting systems. We will use this for the detection of crossings with the Poincaré section as well.

In our simulation code we solve the nondimensional equations. For this we use the physical parameters of the test rig mentioned earlier that was built up in the laboratory. Let us now present some results and in so doing explain some of the particular features of our implementation. Fig. 10(a) shows impacting solutions. The red solution line in the pressure plot is the equidistant cubic interpolation of the solution that can be used for harmonic analysis. An example spectrum of the pressure solution of Fig. 10(a) is presented in Fig. 10(b). The pressure

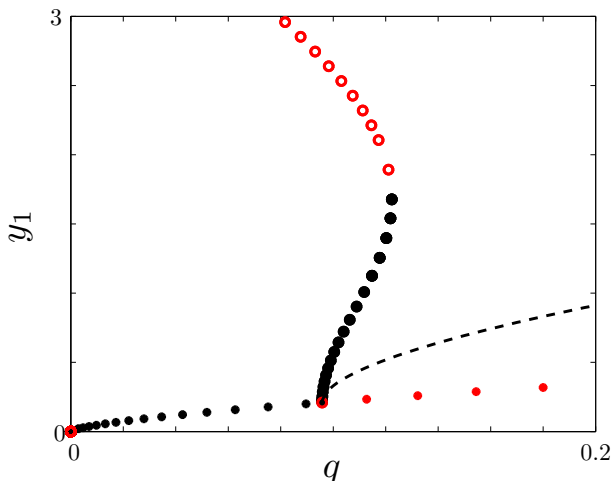


Figure 8: Continuation from the first Hopf point with $\kappa = 0.4$. The stable limit cycle is reaching a fold point, turns back and become unstable. The dashed line represents the analytical estimate.

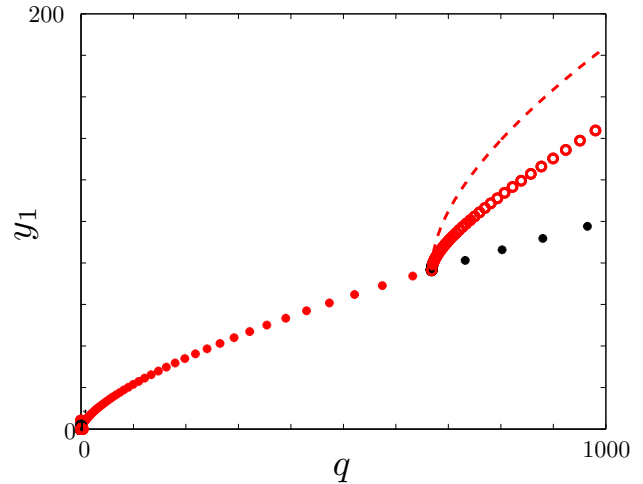


Figure 9: Continuation from the second Hopf point with $\kappa = 0.4$ showing the unstable limit cycle. The dashed line represents the analytical estimation.

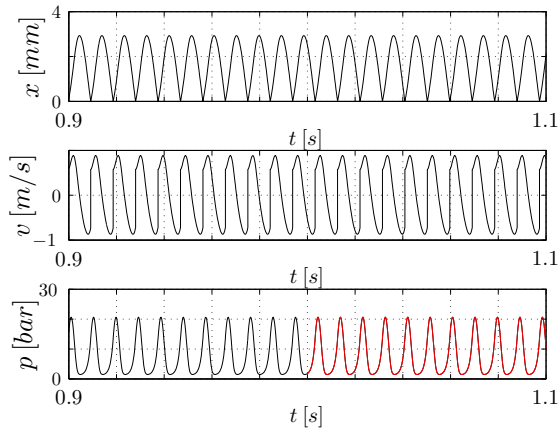
time history is not sinusoidal, so we find higher frequency components as well.

Now let us take a look at the phase space and see the stable impacting limit cycle that exist for particular parameters. This can be seen in Fig. 11. The nondimensional parameters here are $q = 3$, $\kappa = 1.25$, $\beta = 20$ and $\delta = 10$. Our program is capable of treating outer excitation in the form of an explicit time-dependent flow rate disturbance around a given value. This can be useful when comparing numerical and experimental data. The reason of this feature comes from the experiments with the test rig. We experienced that the influence of the periodic excitation of our gear pump unfortunately cannot be neglected. Furthermore, we extended our program with the capability of producing so called *brute force* bifurcation diagrams that will be presented in the next section. These diagrams basically show how trajectory crossings with a given Poincaré section changes when varying a parameter.

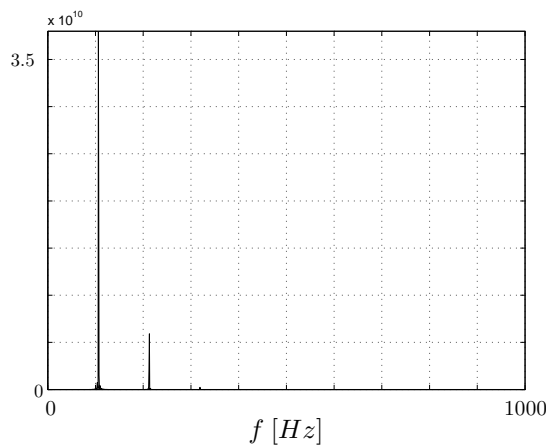
3.2 Numerical bifurcation diagrams

One of the earliest methods we can use during the investigation of dynamical systems is to compute bifurcation diagrams numerically. This can be performed by solving the set of equations with an appropriate ODE solver in forward time. We should choose a suitable Poincaré map in the phase space and let the solution trajectories be recorded when crossing this surface. Starting multiple iterations with random initial conditions for each value of the bifurcation parameter can lead us to the so called ‘Monte Carlo’ diagram.

For all computation the following parameters were cho-



(a)



(b)

Figure 10: A typical impacting solution of the system (a). Displacement (top), velocity (middle) and system pressure (bottom). The spectrum is depicted showing the vibration frequency and its higher harmonical components (b).

sen unless otherwise stated: $\kappa = 1.25$, $\beta = 20$, $\delta = 10$, $r = 0.8$. After an impact the velocity can be written as $v^+ = -rv^-$. Here v^- is the velocity before and v^+ after a particular impact. The bifurcation parameter (the nondimensional flow rate) was varied between $q = 0.01 - 10$ and for each q three random iterations were started from a $30 \times 20 \times 80$ subset of phase space. Figure 12 shows the chosen Poincaré section in the phase space that is simply the $y_2 = 0$ plane.

Now we should take a closer look at the results of the computation that can be seen in Figure 13. There are some interesting regions in the figure that should be discussed. Let us consider reducing q from a high value towards zero. At about $q = 9.18$ a stable limit cycle is born and it grows quick in amplitude with further decrease of the bifurcation parameter. This extreme growth can be explained from the fact that the first Lyapunov coefficient remains relative close to zero but is clearly negative for

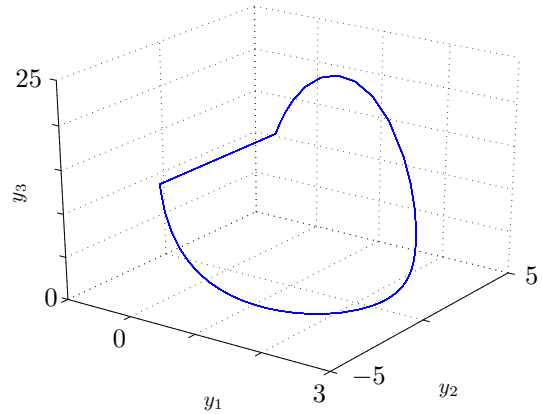


Figure 11: Impacting limit cycle for a nondimensional flow rate of $q = 3$. The constant parameters are $\kappa = 1.25$, $\beta = 20$ and $\delta = 10$.

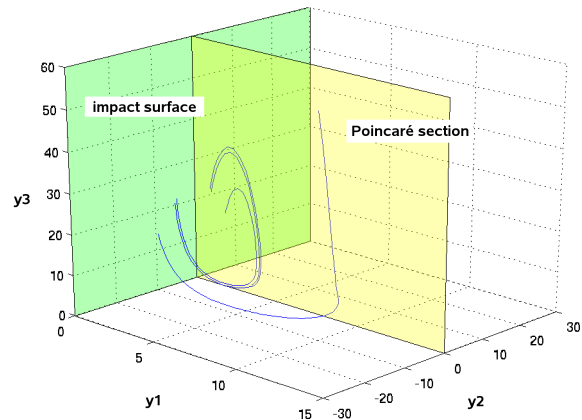


Figure 12: Solution trajectories impacting at the $y_1 = 0$ plane. The yellow plane depicts the chosen Poincaré section, the $y_2 = 0$ plane.

values of q lower than about $q \cong 17338$ as we obtained in subsection 2.3. A typical solution trajectory within this region is depicted in Figure 14(a).

At $q \cong 7.54$ a grazing bifurcation occurs. This means that the amplitude of the vibration grows and reaches the impacting barrier $y_1 = 0$ which means that the displacement x of the valve poppet has reached 0, the value at the valve seat in our physical system. At grazing, only zero velocity impacts occur, this also means that the reset map that is used for determining the velocity after impact is the identity map itself, the velocity before and after the impact are both equal to zero.

With further decrease of the dimensionless flow rate, period-three and period-two impacting solutions can be seen between $q = 6.1 - 7.54$. Parts of this region seem to

be cloudy which is the hallmark of chaotic motion. Figure 14(b) shows an impacting (weakly) chaotic solution. The next interesting point is at $q \cong 5.9$ where a period-two and a period-one impacting solution coexist. The period-two solution is an impacting/grazing one that can be seen in Figure 14(c). This also suggests that another grazing bifurcation occurs in this region when the non-impacting period of the period-two solution touches the impact surface.

Below $q = 5.7$ only a period-one impacting solution exists until $q = 1.4$ where it is clear to see that a so called period-adding cascade starts. Figures 14(d), 14(e) and 14(f) show trajectories corresponding to this region. It is believed that this period adding ends up in the chaos that can be seen on Fig. 15(a). The region below $q = 0.5$

however remains unknown from Fig. 13. The behaviour of the system for these small flow rates is often called *chattering*. In case of chattering a series of impacts occur with less and less valve lift, just like the bouncing ball on a flat surface.

There are basically two types of chattering, *complete* and *incomplete*. At complete chattering an infinite number of impacts occur in finite time and the impacting part will come to a rest, it will *stick*. At incomplete chatter there is no sticking but the impacting body will begin to move for some reason. This can be a force, coming from the rising pressure under the valve poppet in our particular case and this force will lift the poppet again.

There are some issues when modelling the chatter phenomenon and our numerical simulator is not yet able to correctly describe this case and needs improvement. For example we shall consider that our simple impact law may not be valid in this region, when low velocity impacts are following each other quite quick. Also the flow characteristics through the narrowing orifice may change when the poppet is nearing the valve. The pressure will rise when the valve is almost closed and this can have an effect of an additional damping for the system.

All this issues shall be taken into consideration when we wish to investigate the valve's behaviour at low flow rates.

Producing numerical bifurcation diagrams is a very

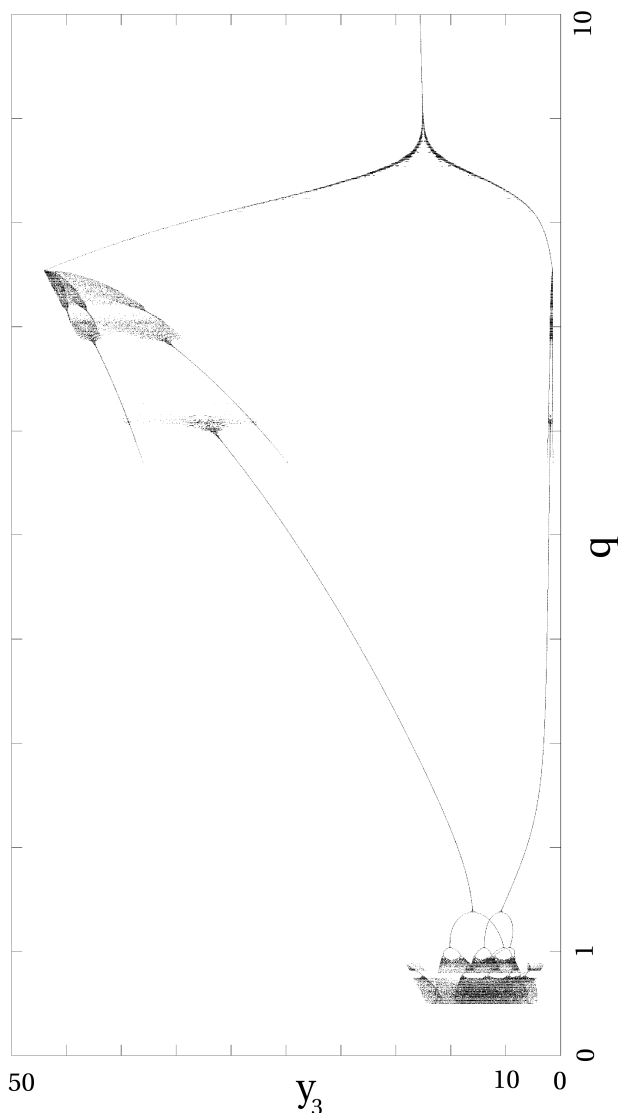


Figure 13: Bifurcation diagram for varying the nondimensional flow rate q . The nondimensional pressure y_3 is plotted against the bifurcation parameter. The other parameters are set to $\kappa = 1.25$, $\beta = 20$ and $\delta = 10$.

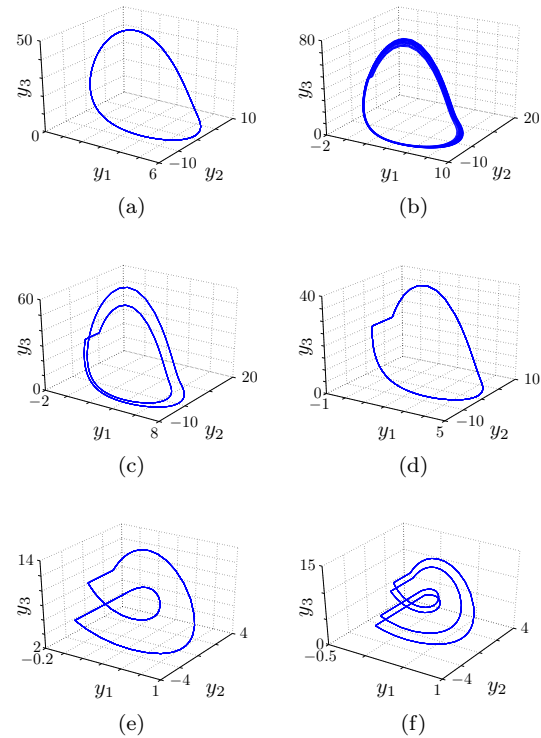


Figure 14: Phase space trajectories along the bifurcation diagram. Non-impacting (a), grazing chaotic (b), period-two impacting/grazing (c), period-one impacting (d), period-two impacting (e) and period-four impacting (f). The parameters are $\kappa = 1.25$, $\beta = 20$ and $\delta = 10$

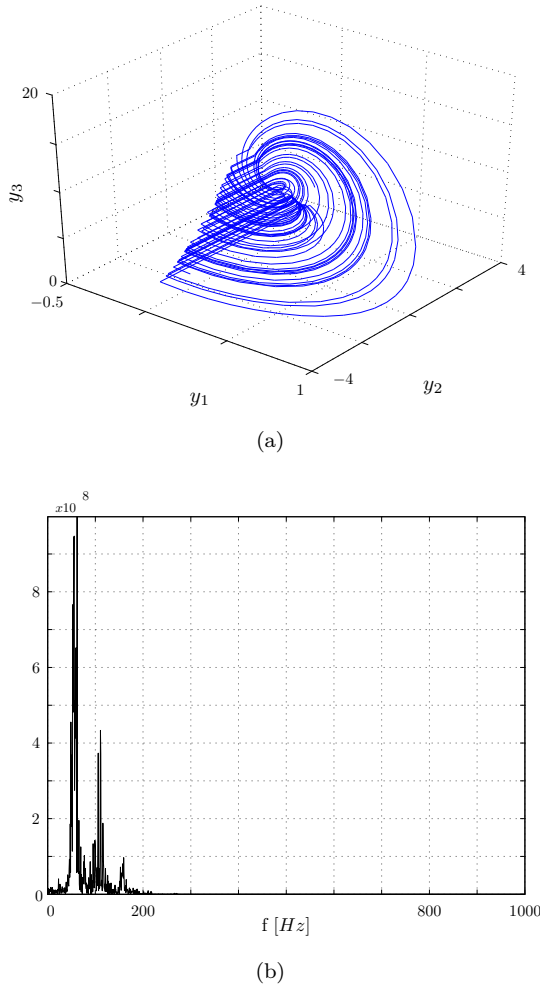


Figure 15: (a) Chaotic attractor for $q \approx 0.85$ with $\kappa = 1.25$, $\beta = 20$ and $\delta = 10$. (b) The frequency spectrum of the solution.

powerful method because these results can give a brief overview of the system's global behaviour. In the next section we will focus on the investigation of the grazing bifurcation that occurs when the response of the system first becomes impacting.

4 Grazing bifurcation analysis

Strong nonlinearities in a dynamical system such as impacts can have serious and sometimes unexpected effects. It sometimes can happen for example that a stable periodic motion will suffer a sudden jump to chaos or at least period adding can be observed. In this section we will use techniques described in [2] to understand more from the discontinuity-induced bifurcations occurring due to grazing of our pressure relief valve with the valve seat.

4.1 Grazing events

In our system for the particular nondimensional parameters used ($\kappa = 1.25$, $\beta = 20$, $\delta = 10$) grazing can occur at two flow rates that are $q = 7.54$ and at $q = 5.95$. The first occurrence is when the period-one nonimpacting limit cycle depicted in Fig. 14(a) touches the impact barrier. The other case is when a period-two limit cycle that already has an impacting period undergo a second grazing (see Fig. 14(c)). In both cases this is character-

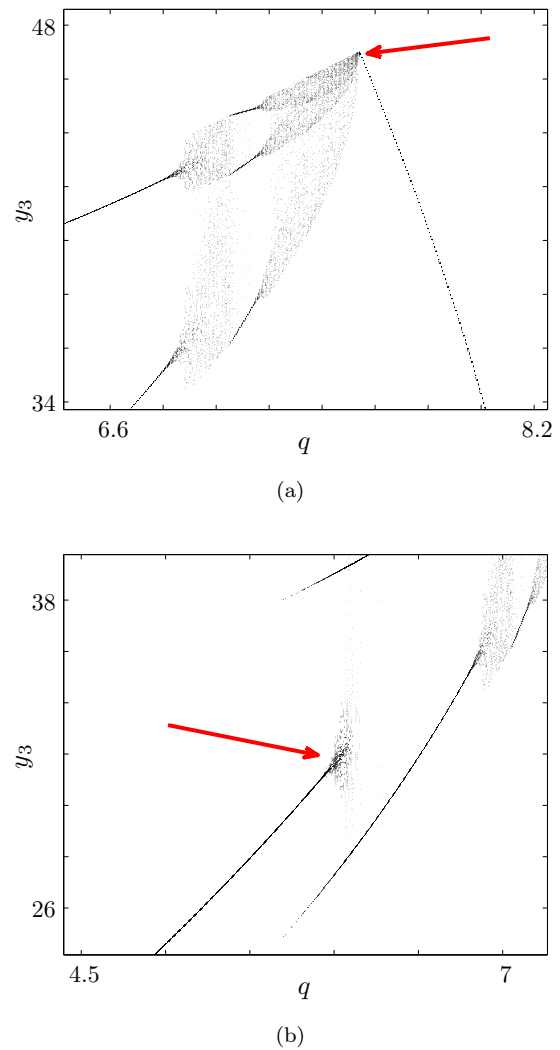


Figure 16: Two grazing events shown in the bifurcation diagram. The first at $q = 7.54$ (a) and the second at $q = 5.95$ (b).

ized by the appearance of a zero velocity impact, however the two grazing events have different effects on the global dynamics. In the first case an immediate jump to chaos can be seen (see Fig. 16(a)) while the second case looks more complicated as depicted in Fig. 16(b).

4.2 Bifurcation scenario at grazing

We carried out an analytical investigation for the first case (where $q = 7.54$) to find out what type of grazing bifurcation we have to deal with. For this we used the theory for nonsmooth systems described in [2]. First we have to find the grazing limit cycle exactly. Our bifurcation diagram in Fig.13 is very helpful, because it contains the critical flow rate q and the nondimensional pressure y_3 can also be obtained. Since we chose the zero velocity plane as our Poincarè section $y_2 = 0$ and at grazing our displacement is also zero. We now have initial conditions that correspond to the last non-impacting limit cycle.

The next step is to solve the so called linear variational equations along the limit cycle, to obtain the *monodromy matrix*. These equations can be written in following form:

$$\dot{w} = \hat{J}w, \tag{14}$$

where \hat{J} is the linear part of the nonlinear system defined in Eq. (5) but without substituting the equilibrium. So (14) can be written in the form:

$$\begin{pmatrix} \dot{w}_1 \\ \dot{w}_2 \\ \dot{w}_3 \end{pmatrix} = \begin{pmatrix} 0 & 1 & 0 \\ -1 & -\kappa & 1 \\ -\beta\sqrt{y_3} & 0 & -\frac{1}{2}\frac{\beta y_1}{\sqrt{y_3}} \end{pmatrix} \begin{pmatrix} w_1 \\ w_2 \\ w_3 \end{pmatrix},$$

and \hat{J} is linear with respect to w . We have to solve (14) together with the system's equations for the period T of the grazing limit cycle three times with the initial conditions $(w_1^{01}, w_2^{01}, w_3^{01}) = (1, 0, 0)$, $(w_1^{02}, w_2^{02}, w_3^{02}) = (0, 1, 0)$ and $(w_1^{03}, w_2^{03}, w_3^{03}) = (0, 0, 1)$. We can then compose the monodromy matrix M from the solution $w(T)$ after one complete period in following way:

$$M = (w^{01}(T) \ w^{02}(T) \ w^{03}(T))$$

We now have to compute the eigenvalues of M and apply the theory described in [2].

For the grazing flow rate $q = 7.54$ we can find $(y_1^0, y_2^0, y_3^0) = (0, 0, 47.07)$ as initial condition of the grazing limit cycle. When we integrate for one period ($T = 2.6547$ for this flow rate) and solve the linear variational equations we obtain that

$$M = \begin{pmatrix} 0.5972 & 0.0450 & -0.0111 \\ 13.4466 & 1.5311 & -0.1306 \\ 40.8328 & 5.1828 & -0.2744 \end{pmatrix},$$

whose eigenvalues are $\nu_1 = 1$, $\nu_2 = 0.8537$ and $\nu_3 = 0$. It is necessary to have one eigenvalue that is equal to 1. ν_3 does not necessarily have to be zero, but presumably it is close to and the difference may be beyond the computation tolerance.

The second eigenvalue gives us important information about the scenario after the grazing event. First of all it has to be less than 1 because the grazing limit cycle is attracting, e.g. it is stable.

According to theory there are three scenarios:

1. If $0 < \nu < 1/4$ then grazing is followed by a period adding, in which the periodic bands overlap,
2. if $1/4 < \nu < 2/3$ then chaotic and stable periodic solutions are alternating and periodic motion forms a period adding cascade,
3. if $2/3 < \nu < 1$ then there is a sudden jump to chaos to obtain, and the chaotic attractor's size is square root proportional to the bifurcation parameter.

Since we have $2/3 < \nu_2 < 1$, a robust chaotic attractor arises, as it can also be seen in Fig. 16(a). It is also easy to notice that it is growing like a square root function. According to literature [2] this behaviour is characteristic to impacting systems. Note that this approach is only valid if we assume that the discontinuity map has quasi one-dimensional behaviour. The literature [2] contains lots of examples and presents various bifurcation diagrams, also ones that refer to the other two scenarios. An example figure for the first case, e.g. when $0 < \nu < 1/4$ looks very similar to our second grazing scenario that arises at $q = 5.95$. This could be analysed with the same technique in a latter investigation.

4.3 The three-dimensional square root map

Impacting systems have a so called square root-type non-linearity. This means that the bifurcation scenario that occur at grazing can be described by a square root map. Such a map can be written in general form

$$x \mapsto Mx + N\mu + Ey, \text{ if } H(x, \mu) < 0, \tag{15}$$

and

$$x \mapsto Mx + N\mu, \text{ if } H(x, \mu) > 0.$$

M is the monodromy matrix mentioned earlier, N is a column vector that is obtained by the same linear variational equations as the matrix M but we have to add the partial derivative with respect to the bifurcation parameter. In our case this only means the addition of β to the third equation since $\frac{\partial y_3}{\partial q} = \beta$. At this time we have to solve the equations around the grazing periodic orbit with the initial conditions $(0, 0, 0)$. In our particular case we obtain

$$N = (0.2269 - 0.1939 - 7.3400)^T.$$

The term Ey in Eq.(15) contains the square root singularity in general and $H(x, \mu)$ in our case is the minimum displacement of the trajectory if we would not allow any impact at all. There are basically two types of discontinuity maps that are used when investigating grazing bifurcations, the *Poincarè-section discontinuity mapping* and the *Zero time discontinuity mapping*. In our investigation we will only focus on the zero time discontinuity map, e.g. *ZDM*. It can be composed by taking an initial

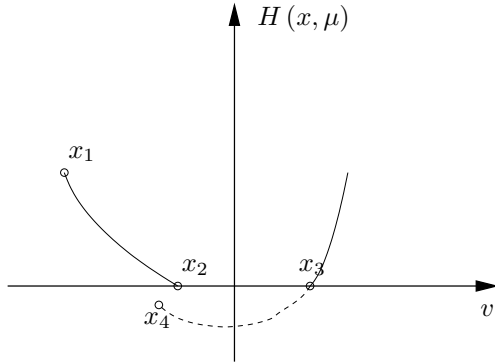


Figure 17: The ZDM maps in practice. The point x_1 is mapped to the point x_4 in which the solution is integrated backward time from x_3 for the time that elapsed between the points x_1 and x_2 .

point arbitrary close to the grazing point and integrating it forward in time until we stop at the impact surface and measure the elapsed time. Then we apply the impact law but this time we integrate backward in time for the same time period that was recorded. See Fig.17 that shows an impacting trajectory together with the important points. For our investigation we will use following analytical approach of the ZDM that can be found in [2]

$$x \mapsto Mx + N\mu, \text{ if } H(x, \mu) > 0 \text{ and}$$

$$x \mapsto Mx + \sqrt{2a^*W(x)}y + N\mu, \text{ if } H(x, \mu) < 0,$$

where a^* is the acceleration at the grazing point, $W(x)$ contains the coefficient of restitution, $\mu = q - q_{crit}$ is the bifurcation parameter and $y = \sqrt{-x}$ represents the square root singularity. In our particular case we can substitute

$$a^* = p^* - \delta \text{ and}$$

$$W(x) = \begin{pmatrix} 0 \\ 1 + r \\ 0 \end{pmatrix},$$

where p^* is the grazing pressure. Next we iterate the three dimensional map and produce bifurcation diagrams by varying the bifurcation parameter. We varied q between 7.4 and 7.6 and obtained the bifurcation diagram for the map presented in Fig.18. It is clear to see that a chaotic attractor arises immediately after grazing. Note that the lower and upper boundaries of the chaotic attractor show linear and square root type shape that is characteristic to impacting systems and the upper square root shaped boundary is proportional to $\sqrt{\mu}$ according to [2].

5 Conclusions

In this paper we presented a mathematical analysis of a simple hydraulic pressure relief valve. We found that

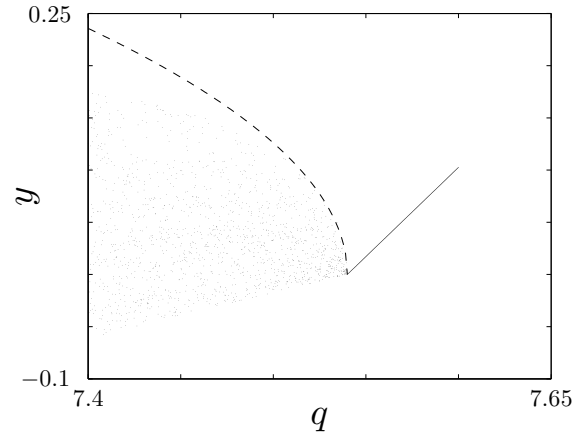


Figure 18: Bifurcation diagram of the three-dimensional ZDM between $q = 7.4 - 7.6$. y is the second coordinate of the map. A sudden jump to chaos can be observed at the critical flow rate $q_{crit} = 7.54$. The dashed line represents the analytical estimation.

these kind of dynamical systems can lose their stability in a particular way in which self-excited limit cycle vibrations occur. We obtained a criterion for stability regarding the flow rate and damping coefficient parameters using linear stability analysis. We have shown that damping of the system has a notable effect on the stability of arising limit cycle.

We also found that for low enough damping, the periodic orbit born in the Hopf bifurcation reaches the valve seat and the system undergoes a grazing bifurcation, with an immediate jump to chaos. We believe that this is the first description of this scenario corresponding to the onset of valve chatter as most previous studies assumed smooth behaviour, and essentially has just found the presence of Hopf bifurcations. As we have shown, the analysis of chatter requires nonsmooth dynamical systems theory.

For very small flow rates, another interesting phenomena occur: as the pressure in the system builds up very slowly, the valve body closes completely, which gives rise to sticking motion. In this case not only impact occurs but for some time intervals (while the valve is shut), the dynamics reduces simply to the pressure dynamics with $x = 0$ and $v = 0$. Our future plan is to analyse this hybrid motion consisting of sticking, impacting and freely oscillating segments. Obviously, laboratory measurements are also needed to verify the theoretical and numerical results.

Acknowledgements. This work was partially supported by the OTKA Grant 76478 of Cs. H6s.

References

- [1] W. Bolton. *Pneumatic and hydraulic systems*. Butterworth-Heinemann, 1997.
- [2] M. di Bernardo, C. J. Budd, A. R. Champneys, and P. Kowalczyk. *Piecewise-smooth dynamical systems*. Springer, 2007.
- [3] E. J. Doedel, R. C. Paffenroth, A. R. Champneys, T. R. Fairgrieve, Y. A. Kuznetsov, B. E. Oldeman, B. Sanstede, and X. Wang. *AUTO 2000 : Continuation and Bifurcation Software for Ordinary Differential Equations*, 2006.
- [4] J. Guckenheimer and P. Holmes. *Nonlinear oscillations, dynamical systems, and bifurcations of vector fields*. Springer, 1983.
- [5] S. Hayashi. Instability of poppet valve circuit. *JSME International Journal*, 38(3), 1995.
- [6] S. Hayashi, T. Hayase, and T. Kurahashi. Chaos in a hydraulic control valve. *Journal of fluids and structures*, (11):693–716, 1997.
- [7] K. Kasai. On the stability of a poppet valve with an elastic support. *Bulletin of JSME*, 11(48), 1968.
- [8] F. X. Kay. *Pneumatics for industry*. The Machinery Publishing Co. Ltd., 1959.
- [9] Yuri A. Kuznetsov. *Elements of applied bifurcation theory*. Springer, 1997.
- [10] H. L. Stewart. *Hydraulic and pneumatic power for production*. The Industrial Press, 1963.
- [11] H. Thomann. Oscillations of a simple valve connected to a pipe. *Journal of Applied Mathematics and Physics*, 1976.